International Journal for Housing Science and Its Applications
Publish August 4, 2025. Volume 46, Issue 3 Pages 1858-1871

https://doi.org/10.70517/ijhsa463147

Research on multi-objective optimal operation and scheduling model of smart microgrid based on mixed integer planning

Yanting Chu[1,3], Yuting Yu[2,3,*], Xiaogui Liu[1], Yixuan Long[1], Yi Zhang[1] and Zhuoxiang Lai[1]

[1] Institute of Railway Power Supply and Electrical Engineering, Hunan Vocational College of Railway Technology, Zhuzhou, Hunan, 412006, China
[2] College of Rail Transit Locomotive and Rolling Stock, Hunan Railway Professional Technology College, Zhuzhou, Hunan, 412001, China
[3] School of Electrical Engineering, College of Engineering, Universiti Teknologi MARA, Shah Alam, 40450, Malaysia

Corresponding authors: (e-mail: chuyanting2008@163.com).

Abstract In this paper, based on the structure of microgrid and the micro power model, the dung beetle optimization algorithm is used to carry out multi-objective optimization of smart microgrid and construct a multi-objective optimal scheduling model. Then, a mixed integer programming method is used to optimize the multi-objective scheduling model and construct a multi-objective optimal scheduling model for microgrid based on mixed integer programming. After example analysis, the optimal operation and scheduling scheme and the economic benefit performance of various types of power supply access are solved. Scenario 2 with a weighting ratio of 0.4/0.6 between the net profit of the microgrid and the fluctuation of the contact line is the optimal operation and scheduling scheme. Compared with wind power access alone, the startup cost of wind-solar complementary access and wind-power-storage integrated access operation is reduced by 13% and 66.1%, respectively, and the operation cost is reduced by 7.53% and 17.2%, respectively, and the change rate of positive spinning standby is 0.6% and 4%, respectively. The integrated wind-optical-storage access can effectively reduce costs and improve economic efficiency.

Index Terms mixed integer planning, multi-objective optimization, smart microgrid, operation scheduling

I. Introduction

With the increasing energy demand and the instability of energy supply, microgrids have attracted widespread attention as a new energy supply model [1], [2]. Microgrid is a new type of network structure, is an effective way to realize active distribution network, by a group of micro power, loads, energy storage systems and control devices constitute the system unit, can realize the load of a variety of energy forms of highly reliable supply [3]-[6]. In order to better realize the efficient operation and reliability of microgrids, this paper proposes a multi-objective optimized operation scheduling method [7].

The multi-objective operation optimization scheduling of microgrids aims to balance the economics, environmental friendliness and reliability of microgrids [8], [9]. Firstly, economy refers to operating the microgrid with minimum cost while satisfying the load demand [10], [11]. This includes choosing appropriate energy supply methods, optimizing energy purchase and sales strategies, etc [12]. Secondly, environmental friendliness refers to reducing carbon emissions and environmental pollution during microgrid operation [13]. This involves optimizing the use and management of energy as well as promoting the development and utilization of renewable energy [14], [15]. Finally, reliability refers to ensuring stable operation of microgrids under various abnormal conditions, which includes fault detection and recovery, planning and utilization of backup energy sources [16], [17].

In this paper, after an in-depth study of the microgrid structure and the micro power model, the multi-objective optimization problem is introduced into the operation of smart microgrids, and the optimization objectives of microgrid operation are realized by using the dung beetle optimization algorithm (DBO) to construct a microgrid multi-objective optimal scheduling model. Then, the microgrid multi-objective optimal scheduling model is optimized by mixed integer programming to construct the microgrid multi-objective optimal operation scheduling model based on mixed integer programming. After example analysis, the best smart microgrid operation and scheduling optimization scheme is solved with full consideration of economy and power fluctuation. Finally, the cost of integrating wind power, photovoltaic and thermal power in the microgrid into the grid is studied to examine the economic benefits of the optimization scheme.

II. Microgrid systems

II. A. Microgrid structure

A microgrid is a small-scale power system [18] that typically includes multiple distributed energy resources, loads, and energy storage devices that can operate independently or be connected to the main power grid. The main objectives of microgrids are to improve the efficiency of energy utilization, enhance the reliability and stability of the power system, and at the same time promote the application of renewable energy and the development of intelligent power systems. Microgrids can be categorized into islanded microgrids and grid-connected microgrids based on how they are connected to the main grid. An islanded microgrid is a microgrid system that is completely detached from the main power grid and operates independently. Independent microgrids are usually applied in remote areas or places that cannot be connected to the main grid, relying on distributed energy sources and energy storage devices to meet power demand, while grid-connected microgrids are microgrid systems connected to the main grid, which can be switched to interconnect with the main grid or independently run according to the needs of the microgrid system, which is usually used in urban and industrial areas, and is able to interact with the main grid when needed to achieve the optimization and flexible dispatching of energy supply. The grid-connected microgrids used in this paper are

The structure of the grid-connected microgrid system used in this paper is shown in Fig. 1, including: photovoltaic modules, wind turbines, diesel generators, micro gas turbines, batteries and loads.

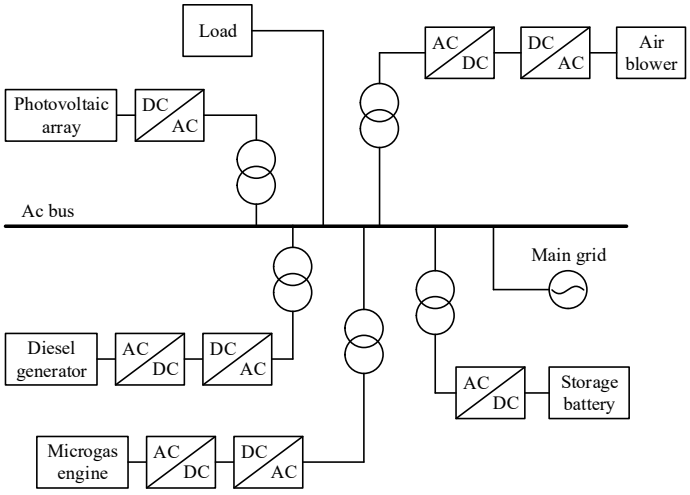

Figure 1: Microgrid model

II. B. Micro power model

II. B. 1) Wind power modeling

A wind turbine is a device that converts wind energy into electrical energy by utilizing a wind wheel or blade to convert wind energy into mechanical energy, and then using the rotation of the rotor to convert the mechanical energy into electrical energy by rotating the rotor's conductive filaments to produce an electric current. In order to maximize the electrical energy, comprehensive consideration must be given to the design of the motor and the control of the magnetic field. Ultimately, by controlling the speed, output voltage and other parameters of the wind turbine, the output power of the wind turbine can be adjusted so that it can meet the requirements of the grid load.

Wind speed plays a decisive role in the output power of wind turbine, and although the wind speed is random and intermittent, through the analysis of a large number of wind speed data, it is found that it satisfies the Weibull distribution curve, and its probability density can be expressed by the following formula (1):

$$f(v)=\frac{k}{v}(\frac{v}{c})^{k-1}e^{-(\frac{v}{c})^{k}} \tag{1}$$

where K is a shape parameter and c is a scale parameter in m/s.

The power characteristic curve of the wind turbine is used to represent the relationship between the output power P_{WT} and the wind speed v, and its functional relationship can be expressed by equation (2):

$$P_{WT}(t)=\begin{cases}0 & v(t)<v_{ci} \text{ or } v(t)>v_{co}\\ a[v(t)^3]+b[v(t)]^2+cv(t)+d & v_{ci}\le v(t)\le v_{ci}\\ P_r & v_r\le v(t)\le v_{co}\end{cases} \tag{2}$$

where $P_{WT}(t)$ is the output power of the WT at the t time slot. a, b, c, and d are the wind speed parameters. v_{ci} is the cut-in wind speed of the WT, v_r is the rated wind speed of the WT, v_{co} is the cut-out wind speed of the WT, and P_r is the rated power of the WT.

II. B. 2) Modeling of photovoltaic power generation

Photovoltaic (PV) power generation is the process of directly converting solar energy into electricity using the photovoltaic effect. When light strikes the surface of a photovoltaic cell, photons excite electrons in the semiconductor material, causing them to jump into the conduction band while forming holes in the lattice. Due to the potential difference between n-type and p-type semiconductors, the electrons and holes will move toward the p-type and n-type semiconductors, respectively, under the action of the electric field, and the metal electrodes will conduct the collected electrons to form an electric current, i.e., the photovoltaic effect. The DC power thus generated can be used to supply electricity directly or stored in a battery for later use. In a photovoltaic system, the output power characteristic curve equation of a photovoltaic cell is shown in equation (3):

$$P_{PV}(t) = P_{STC}\frac{G(t)}{G_{STC}}\left[1 + a_p(T(t) + T_{STC})\right] \tag{3}$$

where $P_{PV}(t)$ is the output power of the PV during the t time period, and P_{STC} is the output power of the PV under standard test conditions. $G(t)$ is the actual intensity of light radiation during the t time period, G_{STC} is the intensity of light radiation under standard test conditions, and a_p is the temperature coefficient of the PV panel. $T(t)$ is the cell temperature at the t time period, and T_{STC} is the PV cell temperature under standard testing.

II. B. 3) Diesel generator model

Diesel generators generate electricity based on the principle of the internal combustion engine by injecting diesel fuel into the cylinder. Inside the cylinder, the diesel fuel is mixed with compressed air to form a combustible gas. This mixture is then compressed, raising its temperature and pressure. At high pressure, the diesel fuel is ignited and combusted, producing high temperature and pressure combustion gases, the release of energy from these combustion gases drives the piston downward. The movement of the piston is converted into a rotary motion by the connecting rod and drives the generator rotor. The rotating motion of the generator rotor creates electromagnetic induction around the wires, which generates alternating current. The process involves multiple conversions of energy, firstly the conversion of chemical energy to thermal energy, then the conversion of thermal energy to mechanical energy, and finally the conversion of mechanical energy to electrical energy, this process realizes the conversion from diesel fuel to electrical energy.

The diesel generator output power can be expressed as:

$$V_{DE}(t) = k_{DE}P_{DE}(t) + l_{DE}P_{DER}N_{DE}(t) \tag{4}$$

where $V_{DE}(t)$ is the fuel consumption of the DE in the t time period, k_{DE} is the slope of the fuel curve, $P_{DE}(t)$ is the output power of the DE in the t time period, l_{DE} is the intercept factor of the fuel curve, P_{DER} is the power rating of a single DE, and $N_{DE}(t)$ is the number of DEs used in the t time period.

II. B. 4) Micro gas turbine model

Micro gas turbine is a small, high-efficiency power generation equipment, the main principle of which is to generate electricity by driving a generator through a turbine with the high-temperature and high-pressure gas produced by gas combustion. It has a high efficiency energy conversion rate and can effectively convert the chemical energy of the fuel into electrical and thermal energy.

The main components of the system include gas supply system, gas combustion system, turbine components, cooling system, exhaust system and control system. The basic working process: firstly, the gas enters the gas combustion system through the gas supply system, and produces high temperature and high pressure gas after combustion, and then turns the generator through the turbine to generate electricity, while the exhaust gas produced is discharged from the system.

The main fuels of the micro gas engine are natural gas and gasoline, and its power-efficiency relationship is shown in Eq:

$$\eta_{MT}(t) = 0.0753\left(\frac{P_{MT}(t)}{65}\right)^3 - 0.3095\left(\frac{P_{MT}(t)}{65}\right)^2 + 0.4174\frac{P_{MT}(t)}{65} + 0.1068 \tag{5}$$

where $\eta_{MT}(t)$ is the operating efficiency of the MT, and $P_{MT}(t)$ is the active output power of the MT at t time.

II. B. 5) Battery model

Battery pack is the core component of microgrid, and its main function is to store the excess power generated by wind turbines and photovoltaic and other power generating equipment at low loads; and release the stored power at high loads to realize the smooth regulation of power demand. It reduces the load pressure and improves the efficiency of electricity consumption during peak hours, and also reduces the impact of grid-connected microgrids on the power grid. If the capacity of the energy storage system is low, it will not only limit the operational efficiency of the microgrid system, but also reduce the reliability of power supply within the system; if the capacity of the energy storage system is too large, it will increase the investment and maintenance costs of the microgrid, and after grid connection, it will also increase the loss of the distribution network, resulting in an increase in the operating costs of the distribution network. Therefore, reasonable configuration of the capacity of the energy storage system can improve the reliability and continuity of microgrid energy supply and realize orderly charging and discharging. When the total output power of the distributed power supply is greater than the total load, the BT charges, and vice versa the BT discharges.

The following are the main performance parameters of the battery:

(1) Charging depth: the ratio of the acceptable power during charging to the capacity at the charging state.

(2) Depth of discharge: the ratio of the discharged capacity to its rated capacity, the deeper the depth of discharge, the shorter the battery life.

(3) Charge state: the size of the charge state describes the remaining capacity compared to the fully charged state, usually expressed as a percentage. The value range is 0 to 1, when SOC = 0 when the battery can not be discharged, SOC = 100 when the battery is fully charged. When 60% $\leqslant$ SOC $\leqslant$ 80%, the battery has the highest discharge efficiency. The battery charging and discharging state is shown in equation (7):

$$I_e = \frac{P_{BT}(t)}{U} \tag{6}$$

$$SOC(t) = \begin{cases} SOC(t-1) + \dfrac{\eta^+ \times I_e(t)}{C_{BT}} & \text{Charge} \\ SOC(t-1) - \dfrac{I_e(t)}{C_{BT} \times \eta^-} & \text{Discharge} \end{cases} \tag{7}$$

where $SOC(t)$ is the remaining capacity of the BT in the t time period, $I_e(t)$ is the charging and discharging current in the t time period, $P_{BT}(t)$ is the power supplied by the storage device in the t time period, and U is the value of the voltage at the two ends of the storage device. C_{BT} is the rated capacity of the BT, and η^+, η^- are the charging and discharging efficiencies, respectively.

III. Multi-objective optimal scheduling model for microgrids based on mixed integer programming

III. A. Multi-objective optimization problem

A multi-objective optimization problem means that multiple objectives need to be solved together when solving a problem [19]. Usually the multi-objective problems are solved by setting a constraint to solve the optimal solution, as shown in Eqs. (8) and (9):

$$\min y = F(x) = \left[f_1(x), f_2(x), \cdots f_{n0.0.}(x)\right], n = 1, 2 \cdots N \tag{8}$$

$$s.t. \begin{cases} g_i \leq 0, i = 1, \\ \quad 2 \cdots m \\ h_i \leq 0, i = 1, 2 \cdots k \\ X = [x_1, x_2, \cdots x_d \cdots x_D] \\ x_{d\min} \leq x_d \leq x_{d\max} d = 1, 2 \cdots D \end{cases} \tag{9}$$

where N refers to the number of all objective functions, $N > 0$ and integer, and F refers to the objective vector to be optimized. X refers to the decision vector, which has dimension D. g_i refers to a set of constraints, and i and m refer to the number of inequality constraints within and across the set, respectively. h_i is a set of constraints identical to the constraints of g_i, i refers to the number of constraints under the same conditions, and the total number of inequality constraints of h_i is k. x_{dmax} and x_{dmin} refer to the upper and lower bounds of all elements in the set of X, respectively.

For a long time, the optimal scheduling problem has been the focus of research by various parties and is very common in various systems.In this paper, the optimization objective of microgrid operation is achieved by Dung Beetle Optimization Algorithm (DBO) [20].

III. B. Multi-objective optimal scheduling model for microgrids

III. B. 1) Microgrid optimal dispatch objective function

The common microgrid components are wind turbines, photovoltaic (PV) generators, diesel generators, micro gas turbines, and energy storage battery systems are five different common power generation units that will be modeled in terms of both economics and environmental protection of the microgrid system, and therefore, the operating costs and environmental protection costs are taken as the objective functions as follows:

(1) Objective Function I: Minimum Operating Costs of Microgrids

The ultimate goal of optimal scheduling is to minimize the cost of operation, which includes the generation cost of each distributed power source, the cost of equipment depreciation, the cost of power purchased from the main grid, taking into account all aspects of spending, as shown in Eqs. (10) and (11):

$$f_1 = \sum_{t=1}^{T} C_{gird}(t) + C_{bess}(t) + C_{MT}(t) + C_{DE}(t) \tag{10}$$

$$\begin{cases} C_{gird}(t) = C_{gird}(t) = C_{buy}(t) + C_{sell}(t) \\ C_{buy}(t) = C_{buy}(t) P_{buy}(t) \\ C_{sell}(t) = C_{sell}(t) P_{sell}(t) \\ C_{DE}(t) = C_{DE.OM}(t) + C_{DE.F}(t) \\ C_{MT}(t) = C_{MT.OM}(t) + C_{MT.F}(t) \end{cases} \tag{11}$$

where $C_{gird}(t)$, $C_{bess}(t)$, $C_{MT}(t)$ and $C_{DE}(t)$ refer to the total cost of the interactions between the microgrid system and the main grid at t, the cost of maintenance required for the normal operation of the BESS, the total operational cost of the MT, and the DE the total operating cost of the MT, and the total operating cost of the DE. $P_{buy}(t)$, $P_{sell}(t)$ denote the power of microgrid system to buy power from the main grid and the power of power to sell power to the main grid at t, respectively. $c_{buy}(t)$, $c_{sell}(t)$ refer to the price of electricity at the time of buying and selling electricity, respectively.

(2) Objective Function II: Minimizing Environmental Protection Costs of Microgrids

China has always adhered to the national policy of protecting the environment, and the construction of any project needs to consider the treatment of pollutants, i.e., the cost of environmental protection, so the less the treatment cost that needs to be consumed for the pollution generated by the project, the better. The specific formula is as (12):

$$\begin{cases} f_2 = \sum_{t=1}^{T} C_{GRID.EN}(t) + C_{MT.EN}(t) + C_{DE.EN}(t) \\ C_{GRID.EN}(t) = \sum_{k=1}^{n} (C_k \gamma_{grid,k}) P_{buy}(t) \end{cases} \tag{12}$$

where $C_{GRID.EN}(t)$ refers to the total cost of the pollutants to be addressed for the amount of electricity purchased by the main grid output microgrid. $\gamma_{grid,k}$ refers to the amount of pollutants of category k produced by the main grid supply, and C_k refers to the cost coefficient of treating pollutants of category k.

(3) Objective Function III: Minimize the total cost of the microgrid

The ultimate goal of optimal scheduling of microgrids is to minimize the total cost, which includes operating costs and environmental protection costs, so the objective function is defined as follows in Equation (13):

$$\min Z = [f_1, f_2] \tag{13}$$

where Z is the total cost of microgrid operation and consumption, f_1, f_2 denote the cost of operation of the microgrid system and the cost of environmental protection, respectively.

III. B. 2) Microgrid optimal dispatch constraints

(1) Power balance constraints:

$$P'_{PV}(t) + P'_{WT}(t) + P_{grid}(t) + P_{DE}(t) + P_{MT}(t) + P_{bess}(t) = P_L(t) \tag{14}$$

(2) Diesel generator output constraints:

$$\begin{cases} P_{DE}^{\min}(t) \le P_{DE}(t) \le P_{DE}^{\max}(t) \\ |P_{DE}(t) - P_{DE}(t-1)| \le r_{DE} \end{cases} \tag{15}$$

(3) Micro gas turbine output constraints:

$$\begin{cases} P_{MT}^{\min}(t) \le P_{MT}(t) \le P_{MT}^{\max}(t) \\ |P_{MT}(t) - P_{MT}(t-1)| \le r_{MT} \end{cases} \tag{16}$$

(4) Transmission power constraints for microgrid systems interacting with the main grid:

$$P_{grid}^{\min}(t) \le P_{grid}(t) \le P_{grid}^{\max}(t) \tag{17}$$

(5) Energy storage battery system lifetime constraints:

$$\begin{cases} P_{bess}^{\min}(t) \le P_{bess}(t) \le P_{bess}^{\max}(t) \\ SOC^{\min}(t) \le SOC(t) \le SOC^{\max}(t) \end{cases} \tag{18}$$

where $P_{DE}^{max}(t)$ and $P_{DE}^{min}(t)$, $P_{MT}^{max}(t)$ and $P_{MT}^{min}(t)$ refer to the upper and lower bounds of the diesel generator outputs and the outputs at the micro gas turbine. r_{DE} and r_{MT} refer to the upper limit of the climbing power at the DE and the micro-MT, respectively, and $P_{grid}^{max}(t)$ and $P_{grid}^{min}(t)$ refer to the upper and lower limits of the transmission power of the microgrid system in its interaction with the main grid. $P_{bess}^{max}(t)$ and $P_{bess}^{min}(t)$ represent the upper and lower limits of the energy storage battery system's output, when the value of $P_{bess}(t)$ is positive, it represents the energy storage battery system power input, and when the value of $P_{bess}(t)$ is negative, it represents the energy storage battery system power output. $SOC^{max}(t)$ and $SOC^{min}(t)$ represent the upper and lower limits of the battery capacity in the storage battery system at t.

III. C. Second-order cone deformation of the optimized model

III. C. 1) Convex optimization problems

Convex optimization has advantages that general mathematical problems do not have [21]. It has a wide range of convergence, can effectively find the global optimal solution, convex optimization outstanding advantages make it become one of the hot issues in the current research in the new situation. Convex optimization problems can be solved by using interior point method or other convex optimization solutions. These solutions can be reliably embedded in computer-aided systems or analytical tools, and can even be used in real-time automated control systems, and there are theoretical advantages of transforming the problem into a convex optimization problem, e.g., the dyadic problem can be interpreted in a new way and solved efficiently.

The general form of a convex optimization problem is shown below:

$$\begin{cases} \min f_0(x) \\ s.t. f_i(x) \le 0, i = 1,2,K,n \\ a_i^T = b_i, 1,2,K,p \end{cases} \tag{19}$$

where f_i is a convex function, the following three aspects need to be satisfied for an optimization problem to be a convex optimization: the objective function of the optimization model is convex, the equation constraints in the optimization model are in affine form, and the inequality constraints are convex. Only when all three conditions are satisfied can the problem be considered as a convex optimization problem. In solving the optimization model, the objective function is minimized by a series of convex transformations, which can be expressed as a level subset of convex inequalities as shown below:

$$\phi(t): R^n \to R \tag{20}$$

where $t \in R$ is a convex function $f_0(x) \le 0 \Leftrightarrow \phi_t(x) \le 0$ that satisfies the following conditions, Eq. x, $\phi_t(x)$ is a non-increasing function of t.

Combining the above formulas, if there is the following problem:

find x

subject to

$$\begin{gathered} \phi_t(x) \le 0 \\ f_i(x) \le 0, i = 0,1,2,K,n \\ Ax = b \end{gathered} \tag{21}$$

The solution of the model can be obtained through Eq. The standard form optimal solution in SOCP is p^* with the following relation $p^* \le t$, and if the model has no solution there is the following relation $p^* \ge t$, and the relation between p^* and a given value can be examined by convexifying the equation conditions and inequality conditions of the model.

Common convex optimization problems include second-order cone planning, semidefinite planning, and least squares planning, among which second-order cone planning has become a trend in the field of optimal scheduling of hybrid AC and DC distribution networks.

III. C. 2) Second-order cone planning

The hybrid AC/DC distribution network optimization model is transformed into a cone model for solving through second-order cone planning [22]. Firstly, the relevant definitions of second-order cone planning are introduced and the standard form of SOCP is shown below:

$$\begin{cases} \min f(x) \\ s.t. Ax = b \end{cases} \tag{22}$$

where the variable $x \in R_N$, the coefficient constants $b \in R_M$, $c \in R_N$, and $A_{M\times N} \in R_{M\times N}$. C is the second-order cone constraint function.

One of the dyadic problems (COD) of second-order cone programming is shown below:

$$(COD) \max \left\{ b^T y \mid A^T y + s = c, s \in K^* \right\} \tag{23}$$

where K is the closed bump cone and K^* is the dyadic cone.

Second order cone:

$$C = \left\{ x \in R_N \mid y^2 \geq \sum_i^N x_i^2, y \geq 0 \right\} \tag{24}$$

Rotate the second order cone:

$$K = \left\{ x \in R_N \mid yz \geq \sum_i^N x_i^2, y, z \geq 0 \right\} \tag{25}$$

Second-order cone programming is efficient in the implementation of the algorithm, and it is not easy to fall into the local optimal solution, which is suitable for the solution of optimization models, and the following focuses on the second-order cone transformation of the model.

III. C. 3) Cone conversion of models

According to the above mixed-integer nonconvex problem model, which is difficult to solve, the original nonconvex model is converted to a standard convex planning model using the second-order cone method in order to solve it efficiently and quickly, and the optimization results are obtained by relaxing and transforming the objective function as well as the constraints in the large-scale optimization model.

(1) Conical transformation of constraints

Since the constraints in the optimization model are not all convex, the quadratic terms and absolute values in the optimization model need to be converted into cones, so that the large-scale non-convex nonlinear model is transformed into a convex planning linear model, which makes the model easier to solve.

1) Second-order cone relaxation of the tidal equations in the hybrid AC-DC distribution network optimization model is performed for the tidal constraints of radial AC distribution network, the tidal constraints of radial DC distribution network, and the tidal constraints of converter station VSC:

$$\text{Define}(I_{ij,t})^2 = \frac{[(P_{ij,t})^2 + (Q_{ij,t})^2]}{(V_{i,t})^2} \tag{26}$$

$$(I_{ij,t}^{DC})^2 = \frac{(P_{ij,t}^{DC})^2}{(V_{i,t}^{DC})^2} \tag{27}$$

Let $I_{ij,t} = (I_{ij,t}^{DC})^2$ and $\dot{V}_{i,t} = (V_{i,t})^2$ substituting into the radial AC distribution network current constraints to obtain the new equation:

$$\tilde{I}_{ij,t} = \frac{(P_{ij,t})^2 + (Q_{ij,t})^2}{V_{i,t}} \tag{28}$$

$$\begin{cases} P_{ij,t} - \tilde{I}_{ij,t} r_{ij} = P_{jk,t} + P_{j,t} \\ Q_{ij,t} - \tilde{I}_{ij,t} x_{ij} = Q_{jk,t} + Q_{j,t} \end{cases} \tag{29}$$

$$V_{j,t} = V_{i,t} - 2(r_{ij} P_{ij,t} + x_{ij} Q_{ij,t}) + [(r_{ij})^2 + (x_{ij})^2] \tilde{I}_{ij,t} \tag{30}$$

Substituting $\tilde{I}_{ij.t}^{DC}=(I_{ij.t}^{DC})^2$, and $\tilde{V}_{i.t}^{DC}=(V_{i.t}^{DC})^2$ into the radial dc distribution network current constraints, we obtain the new equation:

$$\tilde{I}_{ij,t}^{DC}=\frac{(P_{ij,t}^{DC})^2}{\tilde{V}_{i,t}^{DC}} \tag{31}$$

$$P_{ij,t}^{DC}-\tilde{I}_{ij,t}^{DC}r_{ij}^{DC}=P_{jk,t}^{DC}+P_{j,t}^{DC} \tag{32}$$

$$\tilde{V}_{j,t}^{DC}=\tilde{V}_{i,t}^{DC}-2r_{ij}^{DC}P_{ij,t}^{DC}+\tilde{I}_{ij,t}^{DC}(r_{ij}^{DC})^2 \tag{33}$$

Ditto AC distribution network tidal current constraints, substituting to flexible DC device VSC tidal current constraints, substituting to get the new type:

$$\tilde{I}_{ij,t}^{vsC}=\frac{(P_{ij,t}^{vsC})^2}{\tilde{V}_{i,t}^{vsC}} \tag{34}$$

$$\begin{cases}P_{j,t}^{VSC}=P_{i,t}^{VSC}-\tilde{I}_{ij,t}^{VSC}r_{ij}^{VSC}\\ Q_{j,t}^{VSC}=Q_{i,t}^{VSC}-\tilde{I}_{ij,t}^{VSC}x_{ij}^{VSC}\end{cases} \tag{35}$$

The following quadratic equation can be obtained by deforming Eqs. (31) and (34) in a near-relaxation manner:

$$\tilde{I}_{ij,t}\geq\frac{(P_{ij,t})^2+(Q_{ij,t})^2}{V_{i,t}} \tag{36}$$

$$\tilde{I}_{ij,t}^{DC}\geq\frac{(P_{ij,t}^{DC})^2}{\tilde{V}_{i,t}^{DC}} \tag{37}$$

Eqs. (36) and (37) are reduced to the standard second-order cone form:

$$\left\|\begin{matrix}2P_{ij,t}\\ 2Q_{ij,t}\\ \tilde{I}_{ij,t}-V_{i,t}\end{matrix}\right\|_2\leq\tilde{I}_{ij,t}+V_{i,t} \tag{38}$$

$$\left\|\begin{matrix}2P_{ij,t}^{DC}\\ \tilde{I}_{ij,t}^{DC}-\tilde{V}_{i,t}^{DC}\end{matrix}\right\|_2\leq\tilde{I}_{ij,t}^{DC}+\tilde{V}_{i,t}^{DC} \tag{39}$$

When the pulse width modulation method is SPWM $\mu=0.886$, $0\leq M_{i,j}\leq 1$, the new equation is obtained:

$$E_{i,t}\leq 0.5V_{j,t}^{DC} \tag{40}$$

2) Second-order cone relaxation of absolute values and carrying capacity in the hybrid AC-DC distribution network optimization model

The optimization model contains absolute value terms, and second-order cone transformation is performed on the absolute values in the constraints:

For the second-order cone transformation of the absolute values in the ESS of the energy storage device, for the addition of auxiliary variables $\sum_{r=1}^{T-1}\alpha_{i,t}^{ESS}=\sum_{t=1}^{T-1}|u_{i,t+1}^{ESS}-u_{i,t}^{ESS}|$, the following can be obtain the following new equation:

$$\begin{cases}\sum_{t=1}^{T-1}a_{i,t}^{ESS}\leq\lambda_i^{ESS,\max}\\ -\alpha_{i,t}E_{i,t}^{ESS,\max}\leq u_{i,t+1}^{ESS}\leq\alpha_{i,t}E_{i,t}^{ESS,\max}\end{cases} \tag{41}$$

For the second-order cone transformation of the absolute values in the capacitor bank CB, for the addition of the auxiliary variable $\sum_{r=1}^{T-1}\gamma_{i,t}^{CB}=\sum_{r=1}^{T-1}|N_{i,t+1}^{CB}-N_{i,t}^{CB}|$, the following is obtained New equation:

$$\begin{cases}\sum_{t=1}^{T-1}\gamma_{i,t}^{CB}\leq N_i^{CB,\max}\\ B_{i,t}^{CB}\leq\gamma_{i,t}\leq B_{i,t}^{CB}N_i^{CB,\max}\end{cases} \tag{42}$$

Linearization of the formula is carried out using a circle-interconnected square to obtain the new formula:

$$\begin{cases}-\sqrt{2}S_j^{VSC,\max}\leq P_{j,t}^{VSC}+Q_{j,t}^{VSC}\leq\sqrt{2}S_j^{VSC,\max}\\ -\sqrt{2}S_j^{VSC,\max}\leq P_{j,t}^{VSC}-Q_{j,t}^{VSC}\leq\sqrt{2}S_j^{VSC,\max}\end{cases} \tag{43}$$

The quadratic terms $(I_{ij,t})^2,(I_{ij,t}^{pc})^2$ contained in the objective function are replaced by $I_{ij,t},I_{ij,t}^{DC}$, respectively, to obtain the new equation:

$$\begin{cases} C^{ACLoss}=\sum_{t=1}^{T}\sum_{i=1}^{n}\sum_{j=1}^{n}C_t r_{ij} I_{ij,t}\Delta t \\ C^{DCLoss}=\sum_{t=1}^{T}\sum_{i=1}^{n}\sum_{j=1}^{n}C_t r_{ij}^{DC} I_{ij,t}^{DC}\Delta t \end{cases} \tag{44}$$

After convexification of the objective function and constraints as well as linearization the original problem is transformed into a second-order cone planning problem, which is solved efficiently using the well-established second-order cone algorithm.

IV. Example analysis

IV. A. Optimized Solution Solving

In order to reflect the effectiveness of the scheduling optimization model in this paper, the following four scenarios are set up.

Case 1: The traditional power exchange users arrive at the station to change and charge mode, i.e., the optimization of power exchange load scheduling is not considered.

Case 2: Optimization with the goal of maximizing the net profit of the microgrid.

Case 3: Optimization with the objective of minimizing power fluctuation in the contact line.

Case 4: Optimization with the objective of considering the net profit of the microgrid and the fluctuation of the contact line.

Analyzing Case 1, under the traditional mode of arriving at the station and charging at the same time, the power exchange users concentrate on arriving at the station in the 11th, 15th, and 19th time periods, and then immediately charge the replaced batteries, and the power of each load is shown in Fig. 2, which shows that due to the large number of centralized charging of the replaced batteries in the three moments, the total power of the load in the three moments exceeds the upper limit of the interactive power of the contact line (1800 kW), which exceeds the upper limit by 75.54%, 65%, 65%, and 65%, respectively. The maximum peak-to-valley difference of the total load is 3086.48 kW. Therefore, in order to reduce the degree of overrun and the fluctuation of the power of the contact line, the MGT (micro gas turbine) and the ESS (energy storage station) are powered with the maximum power in these three time periods, and the overall operation of the microgrid is shown in Fig. 3, but at this time, the interactive power of the contact line still exceeds its upper power limit by 31.87%, 22.07%, and 20.24%, and the maximum peak-to-valley difference between the contact lines reaches 2,403.56 kW. It can be seen that when the microgrid is centrally connected to the switching loads, if the switching loads are not optimally scheduled, it can only be ensured that the power of the contact lines does not go beyond the limit by restricting the other loads from accessing the microgrid or by increasing the configuration of the energy storage. Analyzing the net profit of the microgrid in Case 1, since both ESS and MGT are at maximum output, the operation and maintenance costs of both are proportional to the output, and the gas turbine still pays more environmental costs, which makes the total cost of the microgrid far more than the total benefit, and finally leads to the net profit of the microgrid of -20,358.67 yuan. Therefore, optimal scheduling of power exchange loads is necessary in terms of both grid security and the microgrid's own economics.

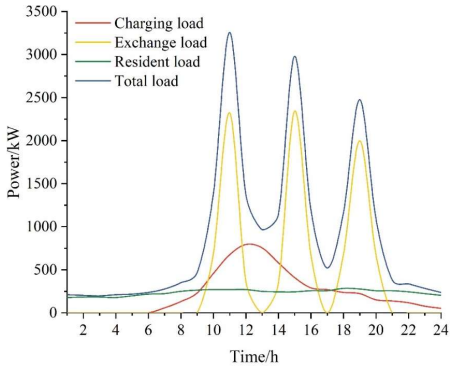

Figure 2: Power curve of each load in Case 1

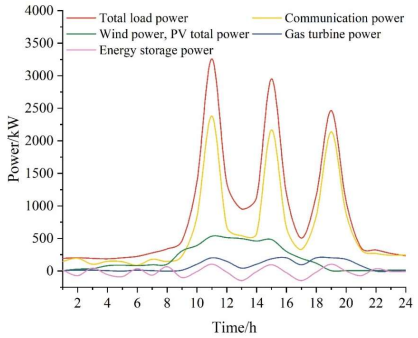

Figure 3: The operation of the microgrid in Case 1

Case 2 With the objective of microgrid obtaining maximum net profit, the microgrid scheduling optimization results are shown in Fig. 4. Analyzing from the perspective of microgrid obtaining the maximum net profit, in order to minimize the cost of power purchase, the time period of BSS (power exchange station) charging the empty batteries are selected in the low time of power purchase tariff, and the cost of operation and maintenance and depreciation of ESS batteries is higher than the gain obtained from discharging the batteries, so the ESS does not choose to charge and discharge the batteries, and the BSS does not discharge the full-charged batteries. MGT has higher operation and maintenance, depreciation cost and environmental cost, so it runs at minimum power throughout the dispatch cycle. From the perspective of contact line power fluctuation, compared with Case 2, the power of the contact line does not exceed the upper limit in one day after optimized scheduling, but the shortcoming is that the contact line power fluctuation is not taken into account, and the maximum peak-to-valley difference of the power on the contact line after scheduling is 1,598.59 kW, with a standard deviation of 617.58 kW, and the peak of the power on the contact line is shifted from the 11th, 15th, and 19th time periods in Case 1 to the 23-5 time periods, the total load mean value is 887.52 kW, and the standard deviation is 532.42 kW, which shows that the BSS plays the role of peak shifting in the microgrid after dispatch optimization.

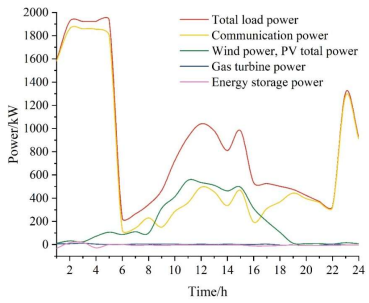

Figure 4: Optimization results of the microgrid in Case 2

Case 3 is optimized with the objective of minimizing power fluctuations on the contact line. To achieve the objective of minimizing power fluctuation of the contact line, Case 3 distributes the centralized switching load to the whole scheduling cycle, with less other loads of the microgrid and more battery charging by the BSS from 1 to 9, while the EV charging loads are larger and less charging by the BSS from 10 to 14, and the calculated mean value of the total load after scheduling is 954.63 kW, with standard deviation 257.13 kW, which is significantly reduced compared to the Case 2's load fluctuation is significantly reduced compared with Case 2. The scheduling optimization results are shown in Fig. 5, which shows that the ESS and distributed energy sources cooperate with each other to share the total microgrid load during the whole scheduling cycle.

Case 4 Considering the two objectives of microgrid net profit and contact line fluctuation, the contact line interaction power of different weighting schemes is shown in Fig. 6. It can be analyzed that, with the gradual increase of the weight of the contact line power fluctuation, the peak-to-valley difference of the contact line power and the standard deviation of the contact line power both decrease, and the contact line interaction power tends to be stable. The decreasing net profit of the microgrid is due to the increase of energy storage plant output to reduce the contact line power fluctuation, whose cost increases more than the reduction of power purchase cost after the contact line fluctuation is reduced, resulting in the net profit still decreasing in the end. Therefore, the net profit of the microgrid and the contact line fluctuation can be considered comprehensively, and the size of the weights of the two can be decided according to the importance of the economy of the microgrid and the contact line power fluctuation.

Combined with the actual operation requirements of the microgrid, the final choice of microgrid net profit and contact line fluctuation weight ratio of 0.4/0.6 of Program 2 is the optimal program under comprehensive consideration.

Table 1: Economic benefit analysis of wind farm operation alone

Time stage	Unit state	Start cost/yuan	Operation cost/yuan	Rotating standby/MW
1	1100000000	0	11025.63	415
2	1100000000	0	12947.52	380
3	1100000000	0	15324.74	240
4	1100000000	0	16893.59	165
5	1100000000	0	17586.49	80
6	1101000000	1560	21896.25	100
7	1101000000	0	20685.05	40
8	1111000000	1525	24986.84	80
9	1111100000	2250	29874.61	98
10	1111110000	540	30897.45	46
11	1111110000	0	30045.78	59
12	1111111000	640	31460.85	97
13	1111110000	0	25034.69	82
14	1111100000	0	22418.57	174
15	1111000000	0	18524.69	144
16	1100000000	0	19435.56	55
17	1100000000	0	19048.62	95
18	1100000000	0	19526.54	15
19	1111000000	2580	25599.54	135
20	1111000000	0	24512.42	25
21	1111000000	0	24512.42	25
22	1101000000	0	22652.16	25
23	1100000000	0	19422.02	50
24	1100000000	0	15789.58	210
Total		9095	520101.61	2835

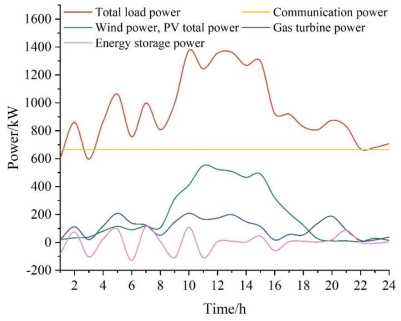

Figure 5: Optimization results of the microgrid in Case 3

IV. B. Analysis of economic benefits

Based on the understanding of the microgrid power structure, this subsection focuses on analyzing the economic benefits of the three types of power sources, namely, wind, light, and storage access and their joint access to the grid. The economic benefits under the separate access of wind farms, wind-solar complementary, and wind-optical-storage joint operation are shown in Table 1, Table 2, and Table 3. Analyzing the above data can be concluded:

(1) When the wind power is accessed alone, in order to ensure that the wind power can be fully consumed, the thermal power unit needs to start and stop frequently, so the start-up cost is higher. When the wind and light complementary system access operation, the thermal power unit start and stop a relatively small number of times, start-up costs reduced by 13%. When the wind - light - storage integrated access operation, the number of thermal power unit start and stop significantly reduced, relative to the wind and light complementary system, start-up costs reduced by 66.1%.

(2) When wind power is connected separately, due to the large fluctuation of the generalized load, in order to meet the constraint of the minimum start-stop time of the thermal power unit, the thermal power unit with a larger minimum specific consumption has to be started, so the thermal power unit has a larger operating cost. When photovoltaic power plants and pumped storage power plants are connected to the system in turn, the generalized load fluctuation gradually smoothes out, the number of thermal power unit startups gradually decreases, and their operating costs are reduced by 7.53% and 17.2% in turn. As can be seen from Table 3, when wind-photovoltaic-storage is accessed and operated as a whole, the main startups with smaller minimum specific consumption are units 1, 2, 3 and 4, and thus the thermal power unit operating costs are relatively small.

(3) When wind power is connected alone, thermal power unit is the only rotating backup of the system, while when PV power station and pumped storage power station are connected to the system, the system rotating backup is in addition to thermal power unit, the remaining output of pumped storage power station and abandoned wind and light can be used as the rotating backup, so the system rotating backup capacity increases, and the rate of change is 0.6% and 4% in turn, in addition to the reliability of the whole system is also improved.

Table 2: Economic benefit analysis of wind and PV operation

Time stage	Unit state	Start cost/yuan	Operation cost/yuan	Rotating standby/MW
1	1100000000	0	11025.63	415
2	1100000000	0	12947.52	380
3	1100000000	0	15324.74	240
4	1100000000	0	16893.59	165
5	1100000000	0	17586.49	80
6	1101000000	1560	21896.25	100
7	1101000000	0	20242.63	58
8	1111000000	1525	22346.15	90
9	1111100000	2250	23467.19	150
10	1111110000	0	23643.48	60
11	1111110000	0	23182.48	88
12	1111111000	0	23643.48	60
13	1111110000	0	22844.95	110
14	1111100000	0	21051.63	105
15	1111000000	0	19423.25	64
16	1100000000	0	16785.48	98
17	1100000000	0	16598.15	104
18	1100000000	0	19526.54	15
19	1111000000	2580	25599.54	135
20	1111000000	0	24512.42	25
21	1111000000	0	24512.42	25
22	1101000000	0	22652.16	25
23	1100000000	0	19422.02	50
24	1100000000	0	15789.58	210
Total		7915	480917.77	2852

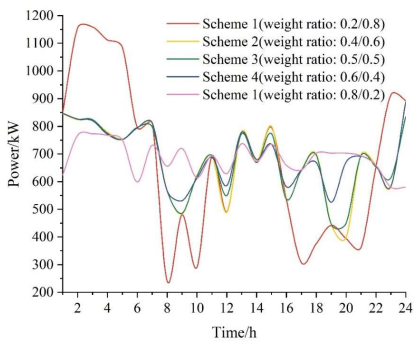

Figure 6: Tie line interaction power under different weighting schemes in Case 4

Table 3: Economic benefit analysis of wind,solar and pumped storage operation

Time stage	Unit state	Start cost/yuan	Operation cost/yuan	Rotating standby/MW
1	1100000000	0	12536.52	240
2	1100000000	0	13526.58	180
3	1100000000	0	15264.32	80
4	1100000000	1560	16248.56	120
5	1100000000	0	17682.61	60
6	1101000000	1525	20642.06	130
7	1101000000	0	19140.24	135
8	1111000000	0	18526.42	140
9	1111100000	0	17356.15	155
10	1111110000	0	20534.23	150
11	1111110000	0	20035.44	125
12	1111111000	0	22145.55	115
13	1111110000	0	20426.71	120
14	1111100000	0	18352.63	145
15	1111000000	0	18422.56	155
16	1100000000	0	18124.02	160
17	1100000000	0	18063.58	155
18	1100000000	0	18415.26	90
19	1111000000	0	18715.63	65
20	1111000000	0	18624.22	60
21	1111000000	0	18704.28	62
22	1101000000	0	18562.42	55
23	1100000000	0	16342.66	120
24	1100000000	0	14248.56	130
Total		3085	430641.21	2947

V. Conclusion

Starting from the microgrid structure and power source composition, the article realizes the optimization objective of microgrid operation by Dung Beetle Optimization (DBO) algorithm, and optimizes the operation and scheduling model by using mixed integer planning. The optimal solution and economic performance are solved through the analysis of arithmetic examples.

In the multi-objective optimization of grid operation scheduling, scheme 2 with a weight ratio of 0.4/0.6 between the net profit of the microgrid and the fluctuation of the contact line is the optimal operation scheduling scheme. Considering the economic benefits of the three power sources of wind power, photovoltaic and thermal power access, the startup cost of wind and solar complementary access operation is 13% lower than that of wind power access alone, and the startup cost of wind-photovoltaic-storage integrated access operation is 66.1% lower than that of wind power access alone. Compared with the operation cost when wind power is connected separately, the operation cost of wind-power complementary access and wind-power-photovoltaic-storage integrated access is reduced by 7.53% and 17.2% respectively. The change rate of positive spinning standby is 0.6% and 4% compared to wind power alone. The wind-photovoltaic-storage integrated access effectively improves the economic efficiency.

Funding

This work was supported by Excellent Youth Project of Scientific Research Project of Hunan Provincial Department of Education (Research on multi-objective optimization operation model for AC/DC hybrid microgrids), grant number 23B1021”.

References

[1] Olivares, D. E., Mehrizi-Sani, A., Etemadi, A. H., Cañizares, C. A., Iravani, R., Kazerani, M., ... & Hatziargyriou, N. D. (2014). Trends in microgrid control. IEEE Transactions on smart grid, 5(4), 1905-1919.

[2] Shuai, Z., Sun, Y., Shen, Z. J., Tian, W., Tu, C., Li, Y., & Yin, X. (2016). Microgrid stability: Classification and a review. Renewable and Sustainable Energy Reviews, 58, 167-179.

[3] Rajesh, K. S., Dash, S. S., Rajagopal, R., & Sridhar, R. (2017). A review on control of ac microgrid. Renewable and sustainable energy reviews, 71, 814-819.

[4] Hooshyar, A., & Iravani, R. (2017). Microgrid protection. Proceedings of the IEEE, 105(7), 1332-1353.
[5] Alzahrani, A., Ferdowsi, M., Shamsi, P., & Dagli, C. H. (2017). Modeling and simulation of microgrid. Procedia Computer Science, 114, 392-400.
[6] Bullich-Massagué, E., Díaz-González, F., Aragüés-Peñalba, M., Girbau-Llistuella, F., Olivella-Rosell, P., & Sumper, A. (2018). Microgrid clustering architectures. Applied energy, 212, 340-361.
[7] López-Prado, J. L., Vélez, J. I., & Garcia-Llinás, G. A. (2020). Reliability evaluation in distribution networks with microgrids: Review and classification of the literature. Energies, 13(23), 6189.
[8] Wang, L., Li, Q., Ding, R., Sun, M., & Wang, G. (2017). Integrated scheduling of energy supply and demand in microgrids under uncertainty: A robust multi-objective optimization approach. Energy, 130, 1-14.
[9] Carpinelli, G., Mottola, F., Proto, D., & Russo, A. (2016). A multi-objective approach for microgrid scheduling. IEEE Transactions on Smart Grid, 8(5), 2109-2118.
[10] Guan, Z., Wang, H., Li, Z., Luo, X., Yang, X., Fang, J., & Zhao, Q. (2024). Multi-objective optimal scheduling of microgrids based on improved particle swarm algorithm. Energies, 17(7), 1760.
[11] Santillán-Lemus, F. D., Minor-Popocatl, H., Aguilar-Mejía, O., & Tapia-Olvera, R. (2019). Optimal economic dispatch in microgrids with renewable energy sources. Energies, 12(1), 181.
[12] Xie, M., Ji, X., Hu, X., Cheng, P., Du, Y., & Liu, M. (2018). Autonomous optimized economic dispatch of active distribution system with multi-microgrids. Energy, 153, 479-489.
[13] Wang, X., Chen, S., Zhou, Y., Wang, J., & Cui, Y. (2018). Optimal dispatch of microgrid with combined heat and power system considering environmental cost. Energies, 11(10), 2493.
[14] Chen, H., Yang, S., Chen, J., Wang, X., Li, Y., Shui, S., & Yu, H. (2024). Low-carbon environment-friendly economic optimal scheduling of multi-energy microgrid with integrated demand response considering waste heat utilization. Journal of Cleaner Production, 450, 141415.
[15] Cheng, S., Su, G. C., Zhao, L. L., & Huang, T. L. (2017). Dynamic dispatch optimization of microgrid based on a QS-PSO algorithm. Journal of Renewable and Sustainable Energy, 9(4).
[16] Sarfi, V., & Livani, H. (2018). An economic-reliability security-constrained optimal dispatch for microgrids. IEEE Transactions on Power Systems, 33(6), 6777-6786.
[17] Lei, B., Ren, Y., Luan, H., Dong, R., Wang, X., Liao, J., ... & Gao, K. (2023). A review of optimization for system reliability of microgrid. Mathematics, 11(4), 822.
[18] Abd El Shafy A. Nafeh,Tarek M.E. Abou Saltouh,Adel A. Abou El Ela & Faten H. Fahmy. (2024). Novel DC-link voltage regulation and seamless transfer control strategy of a battery-based microgrid system. Journal of Energy Storage,86(PB),111352-.
[19] Rohollah Garmanjani,Evelin H. M. Krulikovski & Alberto Ramos. (2025). On Stationarity Conditions and Constraint Qualifications for Multiobjective Optimization Problems with Cardinality Constraints. Applied Mathematics & Optimization,91(1),22-22.
[20] Xiangfei Tao,Kailei Liu,Dong Han,Jing Yang & Hongbin Qiang. (2025). Robust adaptive control with dung beetle optimization algorithm and disturbance observer for load displacement tracking of shock absorber damper test bench. PloS one,20(2),e0314775.
[21] Jiahuan Tang,Chen Ouyang,Hongtruong Pham & Gonglin Yuan. (2025). An inertial Hestenes-Stiefel algorithm for nonsmooth convex optimization and its applications in machine learning. Numerical Algorithms,(prepublish),1-31.
[22] Baha Ulug & Süreyya Akyüz. (2025). Optimized churn prediction using ensemble-based feature selection via second-order cone programming. Annals of Operations Research,(prepublish),1-31.